THE ASTROPHYSICAL JOURNAL, 353:445–451, 1990 April 20

THE NUCLEAR REGION OF NGC 7469

CHARLES J. BONATTO[1] AND MIRIANI G. PASTORIZA[1,2]
Instituto de Fisica, UFRGS, Brazil
Received 1988 February 16; accepted 1989 October 25

ABSTRACT

We have made spectrophotometric observations of the nuclear and circumnuclear regions of the Seyfert 1 galaxy NGC 7469, and we analyze the dynamics and structure of the emission-line regions. In the nuclear region of NGC 7469, we found a broad, an intermediate, and a narrow line-emitting region. The broad lines (FWHM $\approx$ 7800 km s^{-1}) are formed within a distance $R \leq 0.05$ pc from the central source. For the narrow-line region, there is a large range in electron density and a scheme of ionization structure. The circumnuclear stellar population consists mostly of very old stars, and at a distance $R \approx 8''$ from the nucleus, we detected the presence of hot, young stars. The gas at $R \approx 8''$ is nitrogen overabundant.

Subject headings: galaxies: individual (NGC 7469) — galaxies: nuclei —galaxies: Seyfert

I. INTRODUCTION

NGC 7469 is a spiral galaxy with a total magnitude $M_B = 12.8$ and is one of the galaxies with an active nucleus first studied by Seyfert (1943). For the past few years, several spectral regions of NGC 7469 have been extensively surveyed: X-rays (Marshall, Warwick, and Pounds 1981), ultraviolet and optical (De Bruyn and Sargent 1978; Peterson *et al.* 1982), infrared (Rieke 1978), and radio (Ulvestad, Wilson, and Sramek 1981).

Systematic *U*, *B*, and *V* observations show that both the continuum and the emission lines vary in time scales ranging from days to years (Lyutyi 1973, 1977, 1979; Penston *et al.* 1974; Penfold 1979).

Its nuclear spectrum shows broad, very intense, and asymmetric emission lines (Westin 1984, 1985, hereafter We84 and We85). The presence of absorption features, notably Ca II λ3933 K, indicates contamination by the stellar population. The continuum intensity increases blueward, characteristic of a power-law contribution, with a very conspicuous UV bump. A circumnuclear ring of star formation was found from high resolution spectra. Outside the starlike nucleus, high- and low-excitation components were found by mapping the brightest emission lines. Radial expansion is observed for the first component, whereas the latter participates only in the galaxy rotation and is photoionized by hot stars (Wilson *et al.* 1986, hereafter Wi86).

The aim of this work is to investigate the structure of the nuclear and neighboring regions of NGC 7469 in terms of their dynamics and composition by means of the analysis of spectra in the optical region of NGC 7469.

This paper is structured as follows. In § II, we present the observations; the continuum, emission lines, and the kinematics of the nuclear region are analyzed in § III; in § IV, we discuss the emission-line regions; stellar population synthesis and metallicity of the circumnuclear regions are in § V; conclusions are in § VI.

II. OBSERVATIONS

Three spectra of the Seyfert 1 galaxy NGC 7469 were taken with the two-dimensional photon-counting detector "2D-FRUTTI" attached to the Cassegrain focus of the 1 m telescope of the CTIO (Cerro Tololo Inter-American Observatory) on 1986 September 2–5. The slit width was 8″. One spectrum was obtained positioning the slit on the starlike nucleus and summing pixel rows corresponding to 15″ along the slit; the other two were extracted summing pixel rows corresponding to 8″ centered at 5″ north and 8″ south of the nucleus, respectively (Fig. 1). The spectra were reduced using the standard spectrophotometric program TV-RED and were flux calibrated with stars from the catalog "Southern Spectrophotometric Standards" of Stone and Baldwin (1983). The final resolution achieved for these spectra, as estimated from the comparison lamp lines, is of the order of 300 km s^{-1} (FWHM = 5 Å) around $\lambda = 5000$ Å.

The data were corrected for redshift adopting a radial velocity $V_r = 4626$ km s^{-1} as measured from the average value calculated for the narrow forbidden emission lines.

The reddening correction was carried out assuming the interestellar extinction curves given by Seaton (1979) and applying the expression $F_0(\lambda) = F(\lambda)10^{[0.4E(B-V)X(\mu)]}$, where $X(\mu)$ is the extinction function and $\mu = 1/\lambda$, with λ expressed in microns. $X(\mu)$ was expressed as a third-order polynomial fitted to the points of $X(\mu)$ given by Nandy *et al.* (1975). We adopted a color excess $E(B-V) = 0.14$ corresponding to the galactic and internal extinctions to deredden the spectra (We84, We85).

III. THE CONTINUUM AND THE EMISSION LINES

a) *The Continuum*

The stellar contribution was estimated assuming that the absorption spectrum observed at 5″ north of the nucleus represents the average stellar population present in the nuclear region. After subtraction of the emission features from the 5″ north spectrum, the resulting purely absorption spectrum was scaled to 5% of the nuclear spectrum at 5300 Å and then successively subtracted until the nuclear absorption line Ca II λ3933 K disappeared.

A power law ($F_\nu \propto \nu^{-n}$) was fitted to the continuum already free of the stellar contribution in the spectral range $\lambda > 4000$ Å (Fig. 2), and the best result was obtained with $n = 1.0 \pm 0.2$, a typical value for the nonthermal continuum of Seyfert 1 galaxies (Grandi and Phillips 1980; We85; Ferland and

[1] CNPq Fellowship.
[2] Visiting Astronomer at Cerro Tololo Inter-American Observatory.

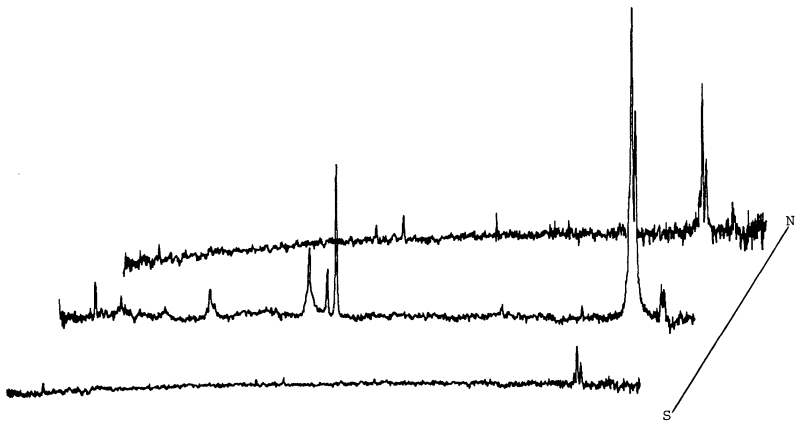

FIG. 1.—The observed spectra according to the positioning of the slit on the galaxy. South is to the bottom, north is to the top; the intensity scale of the off-nuclear spectra was multiplied by 2.

Osterbrock 1987). In the region $\lambda < 4000$ Å, the observed continuum clearly shows an excess over the power-law extrapolation. The stellar, nonthermal, and UV-excess contributions to the observed continuum at three different regions, 3850, 4200, and 5300 Å, are listed in Table 1. For $\lambda > 4200$ Å, the continuum is almost entirely due to the contribution of both the stellar and nonthermal components, but at 3850 Å, this contribution decreases to 78% and the excess dominates shortward of 3850 Å.

b) *Emission-Line Spectrum*

The lines were decomposed using Gaussian profiles by means of a nonlinear least-squares algorithm described in Bevington (1969). The convergence criterium was the minimization of the reduced chi-square χ^2. Using Lorentz profiles as fitting functions always yielded greater χ^2 than Gaussian profiles. Due to the very extended wings and intense core, the H I Balmer lines were fitted with three distinct Gaussian components each: a narrow one with FWHM ≈ 450 km s^{-1}, an intermediate one with FWHM ≈ 2380 km s^{-1}, and a broad one for the base with FWHM ≈ 7830 km s^{-1}. The Gaussian components used to fit Hα were constrained to appear in the fit of the other H I lines with the same FWHM (km s^{-1}) as the corresponding component in Hα. [O III] λλ4959, 5007 and [Ne III] λλ3869, 3968 also show broad bases and intense cores and were fitted with two Gaussians. A blue asymmetry is observed in the base of the [O III] λλ4959, 5007 pair, in opposition to the red asymmetry of the H I lines. The [O III] lines have been constrained to the theoretical ratio of 2.9. Figure 3 shows the result of this procedure for the Hβ + [O III] region.

We present in Table 2 the intensity (or total flux) I, the FWHM, and the emission velocity V_{em}; the error (σ) in the intensity was estimated according to the noise level around each line.

The broad components of the H I Balmer lines exhibit a high emission velocity with a mean value of $\langle V_{em} \rangle = 1017 \pm 300$ km s^{-1}; the intermediate components of the H I lines and the broad components of [Ne III] λλ3869, 3968 have $\langle V_{em} \rangle = 260 \pm 75$ km s^{-1}, whereas the broad components of [O III] λλ4959, 5007 have a negative emission velocity $V_{em} = -150$ km s^{-1}. The narrow components of all the lines do not show any appreciable emission velocity.

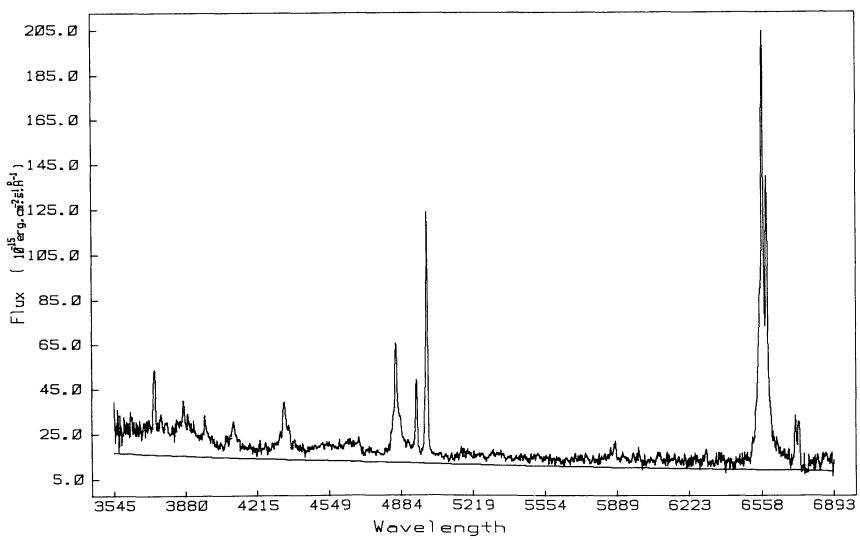

FIG. 2.—Power-law ($F_\nu \propto \nu^{-1}$) fit to the nuclear continuum of NGC 7469 after the subtraction of the stellar contribution. A suitable constant was added to the power-law curve for ease of visualization.

TABLE 1

RELATIVE CONTINUUM CONTRIBUTIONS

Component	3850 Å	4200 Å	5300 Å
Stellar	35	47	50
Nonthermal	43	45	46
UV-Excess	22	8	4

We present in Table 3 the contribution of each component to the total luminosity of the Balmer lines. It is interesting to point out that the intermediate component contributes about 50% for all the lines.

c) *Kinematics of the Nuclear Region*

The turbulence velocity V_t, defined as FWHM/1.67, is plotted in Figure 4 against V_{em}, showing a correlation that suggests the existence of three regions with different kinematic properties. The broad components are formed in a region close to the central ionizing source with the highest turbulence velocity ($\langle V_t \rangle = 4690 \pm 31$ km s^{-1}) and with $\langle V_{em} \rangle = 1017 \pm 300$ km s^{-1}. In the intermediate-line region (ILR), we measured $\langle V_{em} \rangle = 260$ km s^{-1}. The gas and dust present in the narrow-line region participate, on average, in the global rotation of the galaxy, as also shown by Wi86.

IV. DISCUSSION

Assuming that lines with similar FWHM values are emitted by gas with similar conditions, the decomposition of the emission lines in distinct components can be used to derive physical parameters for each emitting region.

a) *BLR and ILR*

For the broad and intermediate components, the Balmer decrement seems to be due mostly to recombination processes. As for the narrow component, this is also valid only assuming a strong absorption by dust, as shown in Figure 5. This fact allows one to estimate the BLR radius and the mass of ionized gas in the BLR and ILR (Osterbrock 1978).

Using the result that the Hβ luminosity comes from recombination and $\langle N_e \rangle = 10^9$ cm^{-3} as a representative value of the electron density in the BLR (because no forbidden line is observed with FWHM similar to the broad H I lines), and $\langle N_e \rangle = 10^6$–$10^8$ cm^{-3} for the ILR ([Ne III] and [O III] have FWHM values similar to the intermediate H I components), then $14 < M_{ILR}/M_{BLR} < 1400$. The mass in the BLR can be estimated using $M_{BLR} = (N_p M_p + N_{He} M_{He}) V \epsilon$, and $L(\mathrm{H}\beta) = N_e N_p \alpha(\mathrm{H}\beta) V \epsilon h\nu(\mathrm{H}\beta)$. With 97.14 Mpc as the distance of NGC 7469 ($H_0 = 50$ km s^{-1} Mpc^{-1}), and a normal helium density $N_{He} = 0.1 N_p$, we have $M_{BLR} \approx 9.2\ M_\odot$, and $130 < M_{ILR} < 13{,}000\ M_\odot$. From the variability of the O IV λ1549 line (We84, We85) and assuming spherical symmetry, we derive $R_{BLR} \approx 6.2 \times 10^{16}$ cm, and with the above mass estimate, $\epsilon \geq 10^{-3}$.

b) *NLR*

De Robertis and Osterbrock (1984) showed that for many high-ionization Seyfert nuclei, there exist good correlations between emission-line width with the ionization potential (IP) and with the critical density for de-excitation (N_c). In Figures 6 and 7, respectively, we plotted FWHM against IP and FWHM against log (N_c) for the narrow lines. These figures imply that the NLR of NGC 7469 is formed by a series of clouds of gas, each of which has a wide range of ionization zones, but in which the denser clouds are, on average, closer to the central ionizing source and move with a larger velocity dispersion than the less dense ones. For the ILR, a strong correlation of FWHM and log (N_c) was found.

For the low-ionization species, the electron density was obtained using the observed line ratios [S II] λ6717/λ6731, [S II] $\lambda\lambda$4068, 76/$\lambda\lambda$6717, 31, and [N II] $\lambda\lambda$6548, 84/λ5755 (Table 2), together with the theoretical curves for these line ratios given by McCall (1984) (Fig. 8), and assuming a canonical electron temperature $T_e = 10^4$ K; we found, respectively, $N_e = (7.1 \pm 0.2) \times 10^2$ cm^{-3}, $(2.7 \pm 0.2) \times 10^3$ cm^{-3}, and $(9.4 \pm 1.4) \times 10^4$ cm^{-3}. Thus, for these ions, the electron density is in the range $700 \leq N_e \leq 10^5$ cm^{-3}.

Density has also been derived from the [O III] lines considering two cases: (*a*) [O III] λ4363 also has a broad component

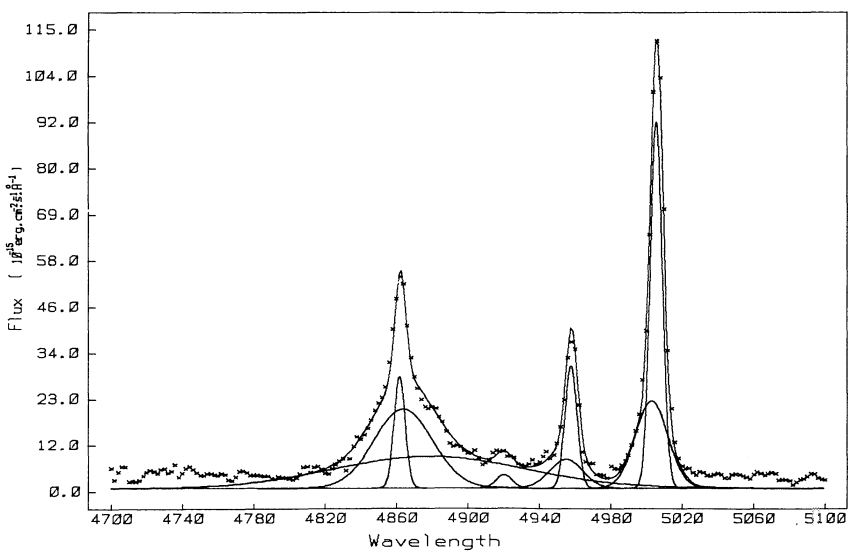

FIG. 3.—Gaussian decomposition of the Hβ + [O III] profile; two components were used to fit each line of the pair [O III] $\lambda\lambda$4959, 5007

TABLE 2

EMISSION-LINE PARAMETERS

Ion	λ_0	I (10^{-15} ergs cm^{-2} s^{-1})	σ	FWHM (km s^{-1})	V_{em} (km s^{-1})	Ion	λ_0	I (10^{-15} ergs cm^{-2} s^{-1})	σ	FWHM (km s^{-1})	V_{em} (km s^{-1})
[O II][a]	3727	350	25	912	647	[Ne IV]	4720	21	8	439	174
H9	3835	57	20	726	695	[Fe III]3F ...	4755	20	10	594	106
[Fe V]	3851	56	20	723	255	[Fe II]20F ..	4774	21	7	444	63
[Ne III]i	3869	169	37	1441	207	[Fe II]20F ..	4815	26	7	424	120
[Ne III]n	3869	50	14	566	219	Fe II 30	4826	26	8	463	145
H8 + He I ..	3889	70	13	563	165	(Hβ)b	4861	638	127	7856	1160
[Fe V]	3896	26	9	397	193	(Hβ)i	4861	889	38	2375	254
[Ne III]i	3969	93	32	1442	364	(Hβ)n	4861	208	7	451	128
[Ne III]n	3969	38	12	552	80	He I	4914	31	7	451	221
Hε	3970	94	60	2669	605	Fe II	4922	26	8	534	208
Fe II 172	4044	25	12	594	231	[O III]i	4959	166	19	1308	−152
[S II]	4068	40	10	490	3	[O III]n	4959	258	7	482	15
[S II]	4076	37	10	489	0	[O III]i	5007	500	19	1295	−150
(Hδ)b	4101	169	158	7752	658	[O III]n	5007	775	7	477	15
(Hδ)i	4101	272	48	2388	315	[Fe VI]	5147	21	5	368	17
(Hδ)n	4101	33	9	534	234	[Fe VII]	5158	48	8	518	116
Fe II 12	4251	37	13	620	157	[Fe VI]	5177	42	7	457	130
Fe II 27	4303	21	12	580	152	[Fe VI]	5678	17	8	365	58
(Hγ)b	4340	307	159	7856	848	He II	5694	32	9	417	36
(Hγ)i	4340	454	48	2391	318	[Fe VII]	5721	48	15	682	68
(Hγ)n	4340	79	9	505	120	[N II]	5755	39	15	629	63
[O III]	4363	49	11	588	209	(He I)i	5876	347	110	4699	−457
[Fe II]	4451	17	7	370	168	(He I)n	5876	60	12	500	152
He I	4471	31	10	553	160	Fe II 46	5991	58	13	528	91
Fe I 2	4482	49	14	747	157	[Fe VII]	6085	116	24	981	−60
Fe II	4500	53	18	948	153	Fe II 74	6248	45	13	526	88
Fe II 37 38 ...	4512	30	10	536	89	[O I]	6300	91	15	539	123
Fe II 37	4520	48	10	547	133	[O I]	6364	44	9	306	−18
Fe II 39	4531	34	8	454	145	[N II]	6548	253	12	394	99
Fe II 38	4541	48	10	509	55	(Hα)b	6563	1624	240	7863	1405
Fe II 186	4549	43	8	446	154	(Hα)i	6563	2843	72	2377	158
Fe II	4559	34	9	465	33	(Hα)n	6563	1419	13	451	92
Fe II 38	4576	33	10	550	220	[N II]	6584	760	12	392	76
Fe II 54	4628	58	11	626	75	[S II]	6717	246	16	489	29
He II	4686	105	14	787	220	[S II]	6732	248	16	488	45

NOTES.—Letters "b," "i," and "n" refer to the broad, intermediate, and narrow components.

[a] Blend of [O II] λ3726 and [O II] λ3729.

but it cannot be detected; using only the narrow components in the ratio $R = [O\ III]\ \lambda\lambda 4959, 5007/\lambda 4363$, we found $N_e = (2.1 \pm 0.3) \times 10^6$ cm^{-3}; and (*b*) the two components of [O III] λλ4959, 5007 and the one of [O III] λ4363 are emitted by gas with, on average, similar conditions, then $N_e = (1.2 \pm 0.1) \times 10^6$ cm^{-3}. Under the conditions of case (*b*), the observed ratio $R \approx 35$ cannot be reproduced for $N_e < 10^5$ cm^{-3} unless $T_e > 18{,}000$ K, a value too high for the NLR of Seyfert 1 galaxies (Filippenko and Halpern 1984). This situation is even more critical in case (*a*). The critical density of [O III] λ4363 is 3.3×10^7 cm^{-3}, whereas for [O III] λλ4959, 5007 $N_c = 7.9 \times 10^5$ cm^{-3}. In fact, [O III] λ4363 is broader than [O III] λλ4959, 5007 by about 100 km s^{-1}, implying that $N_e \geq 10^7$ cm^{-3} in the clouds that produce most of the [O III] λ4363, whereas $N_e \leq 10^6$ cm^{-3} in the clouds that produce most of the [O III] λλ4959, 5007. Also, gas with $N_e \geq 10^7$ cm^{-3} must enhance the Balmer lines relative to [O III] λλ4959, 5007, because the N_c value for the Balmer lines is much higher. The ratio [O III] λλ4959, 5007/Hβ ≈ 5 is much smaller than the typical range 10–20 usually found in NLR of Seyfert 1 galaxies (Koski 1978).

The above results clearly show that the density in the NLR of NGC 7469 varies from $N_e \approx 700$ cm^{-3} up to $N_e \approx 10^7$ cm^{-3}, and they also give support to the idea of an ionization structure for the NLR.

TABLE 3

RELATIVE CONTRIBUTION OF BALMER COMPONENTS

Line	Broad	Intermediate	Narrow
Hα	28	48	24
Hβ	37	51	12
Hγ	36	54	10
Hδ	36	57	7

TABLE 4

EQUIVALENT WIDTH OF ABSORPTION LINES

Line	5″ North (Å)	8″ South (Å)
H8 λ3835	6.93	2.68
Ca II λ3933 K	6.70	5.24
Hε + Ca II λ3970 H ...	6.92	7.09
Hδ λ4101	1.92	3.39
G band λ4300	2.97	...

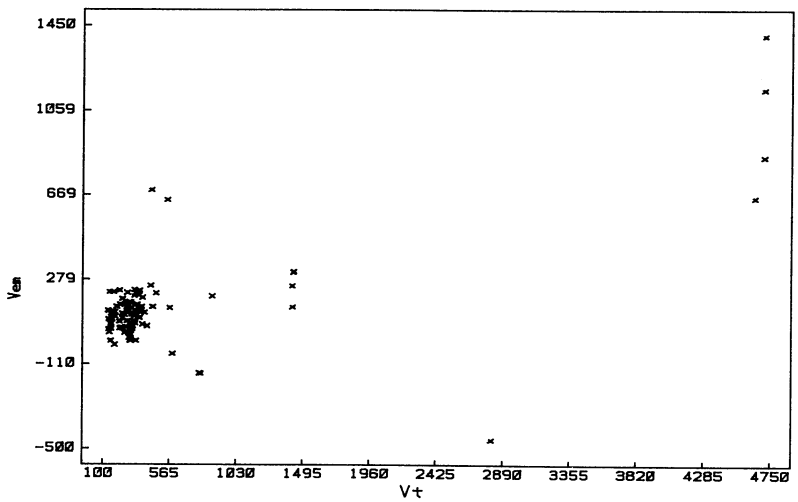

FIG. 4.—Distribution of the emission velocity (V_{em}) against the turbulent velocity (V_t). V_{em} and V_t are in km s^{-1}.

V. CIRCUMNUCLEAR REGIONS

Spectroscopic, IR, and radio observations of the outer regions of NGC 7469 show the existence of an extended high-ionization gas component surrounded by a ring of H II regions at a distance of about 10″ from the nucleus (Wi86). We use our off-nuclear spectra to add new information on the stellar population and metallicity of these regions.

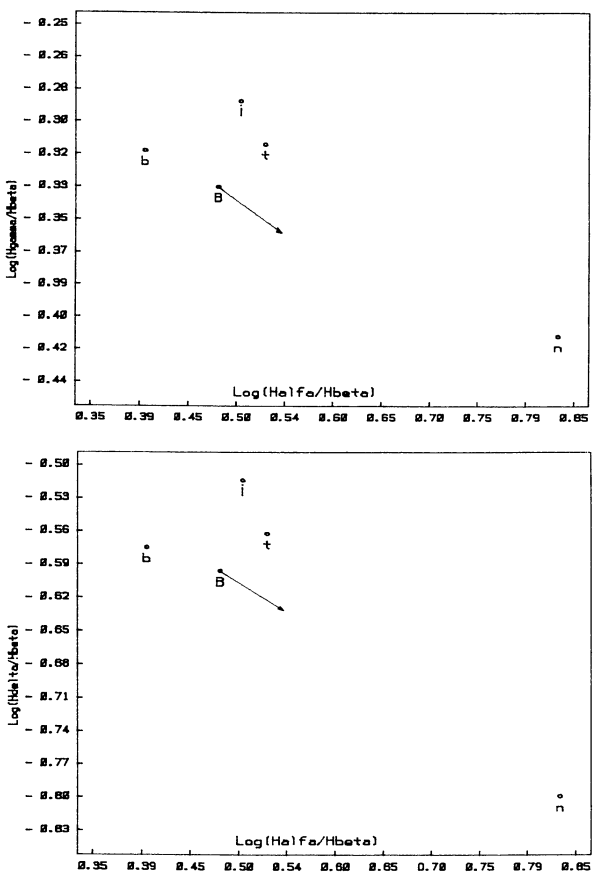

FIG. 5.—Balmer decrement. Lower case "b," "i," and "n" refer to the broad, intermediate, and narrow components of the H I Balmer lines; t is the total Balmer decrement; B refers to the case B value of the recombination theory; the arrow indicates the reddening effect for $E(B-V) = 0.14$. *Top panel*: log (Hγ/Hβ) × log (Hα/Hβ); *bottom panel*: log (Hδ/Hβ) × log (Hα/Hβ).

The 5″ north and 8″ south spectra are clearly contaminated by the underlying stellar population (Fig. 1), which allows us to study the stellar content around the starlike nucleus. The equivalent width of the most prominent absorption lines (Table 4) together with the continuum shape were used to determine the corresponding stellar population templates, selected from a library built from star clusters spectra collected with IDS and CCD detectors at the ESO 1.5 and 2.2 m telescopes (for details, see Bica 1988 and references therein). According to that synthesis model (S4), the stellar population contribution at 5870 Å to the 5″ north spectrum is more than 80%, due to very old stars ($>5 \times 10^9$ yr), and the remaining contribution comes from intermediate and moderately young stars ($>10^8$ yr). For the 8″ south spectrum, the model template (S6) predicts a very old star contribution of 70% and an excess population of stars with $10^6 <$ age $< 10^8$ yr with respect to that at 5″. In Figure 9, we show the 8″ south spectrum, its template, and the subtraction. The maximum metallicity attained by the models is solar (Bica 1988).

After subtracting the templates, we measured the intensity of the emission lines on the pure emission spectra (Table 5). Intensity ratios plotted on the BPT diagrams (Baldwin, Phillips, and Terlevich 1981) unambiguously show that the 5″ north region is photoionized by a power law and should be the high-excitation component that was also found in Wi86. The 8″ south spectrum is typical of an H II region, in agreement with the young stellar population found in the population synthesis.

The metallicity of the 8″ region was inferred from intensity ratios of the observed lines using the diagrams 13*a* and 13*c* in Dopita and Evans (1986). Using their Table 1, we found $12 + \log (O/H) = 8.83$, roughly the solar value, and we derive an N/O abundance $\log (N/O) = -0.85$, nearly twice the solar value. In the diagram $\log (N/O) \times 12 + \log (O/H)$ in Pagel and Edmunds (1981), the position of the 8″ H II region also indicates an N/O ratio above solar.

Basically, our results agree with those of Wi86 and are reinforced by the presence of a young stellar population as derived by the population synthesis and the finding that the gas in the 8″ H II region is nitrogen enriched by secondary mechanisms.

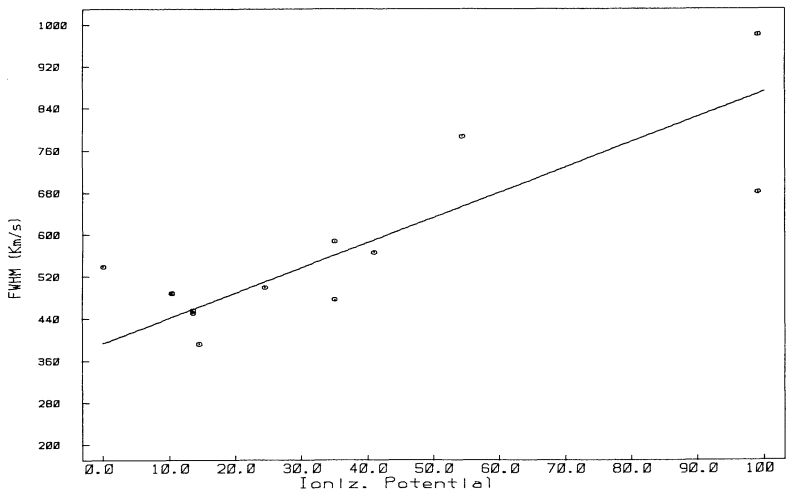

FIG. 6.—Correlation between the FWHM (km s^{-1}) and IP for the narrow lines; the linear correlation is given by FWHM = 4.79 IP + 393.61, and the correlation coefficient is $R^2 = 0.9$.

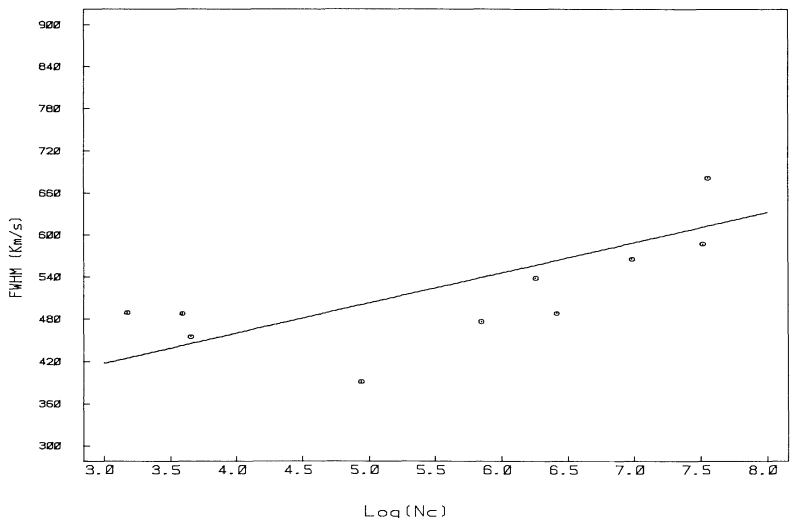

FIG. 7.—Correlation between the FWHM (km s^{-1}) and log (N_e) for the narrow lines; the equation of the line is FWHM = 43.06 log (N_e) + 288.33, and $R^2 = 0.78$.

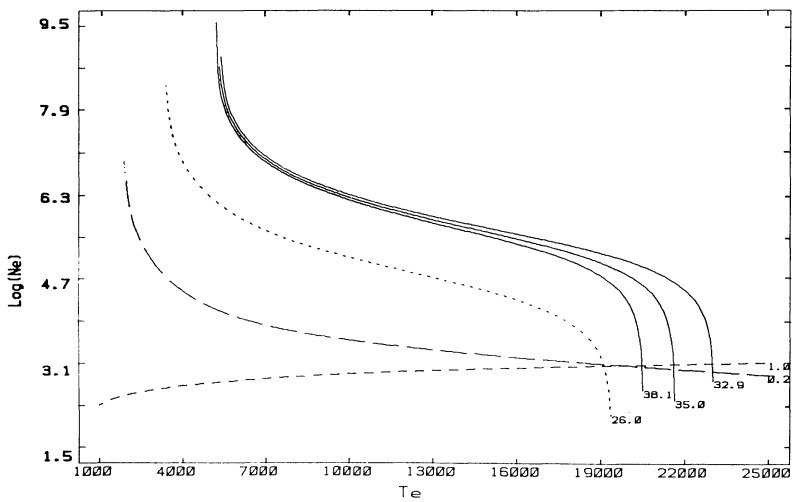

FIG. 8.—Relations between N_e and T_e. Solid lines show the behavior of R = [O III] $\lambda\lambda$4959, 5007/4363; dotted line shows [N II] $\lambda\lambda$6548, 6584/5755; short-dashed line shows [S II] λ6717/6731; and long-dashed line shows [S II] $\lambda\lambda$4068, 4076/6717, 6731. For the [O III], we plot curves for the mean and the extreme values of R.

TABLE 5

OFF-NUCLEAR EMISSION-LINE PARAMETERS

Ion	λ_0	5″ North FWHM (km s^{-1})	5″ North Flux (10^{-15} ergs cm^{-2} s^{-1})	8″ South FWHM (km s^{-1})	8″ South Flux (10^{-15} ergs cm^{-2} s^{-1})
[O II]	3727	430	28 ± 3	605	169 ± 13
[Ne III] ...	3869	...	...	783	74 ± 18
Hβ	4861	634	61 ± 3	389	82 ± 5
[O III]	4959	579	29 ± 3	464	28 ± 5
[O III]	5007	573	87 ± 4	460	87 ± 5
[N II]	6548	537	90 ± 14	455	113 ± 38
Hα	6562	379	377 ± 10	377	602 ± 31
[N II]	6584	534	271 ± 14	452	338 ± 38
[S II]	6717	223	48 ± 10	370	86 ± 35
[S II]	6731	223	33 ± 10	370	99 ± 35

This fact could be assigned to supermassive stars associated with star-forming events occurring during the last 10^8 years.

VI. CONCLUSIONS

The main conclusions of our work can be summarized as follows. From the analysis of the emission lines, we found that in the nuclear region of NGC 7469, there exist at least three emission-line regions with distinct physical parameters, mainly the electron density and temperature. The BLR has a typical dimension of $R \approx 10^{17}$ cm. For the NLR and the ILR, we observed a strong correlation between the FWHM and N_c, which can be viewed as the result of an ionization structure scheme holding in these regions. The interval in electron density shows the coexistence of clouds spanning a large range in density in the NLR.

The circumnuclear stellar population consists mostly of very old stars ($> 10^{10}$ yr) having superposed a conspicuous ring of stars younger than 10^8 yr at $R \approx 8''$. The presence of hot, young stars in these regions is further confirmed by dust emission in 3.3 μm (Cutri *et al.* 1984) and by the steep far-infrared continuum (Wi86). This picture is consistent with the emission spectra of gas still photoionized by the central source at $R \approx 5''$, whereas hot stars photoionize the nitrogen-enriched gas at $R \approx 8''$.

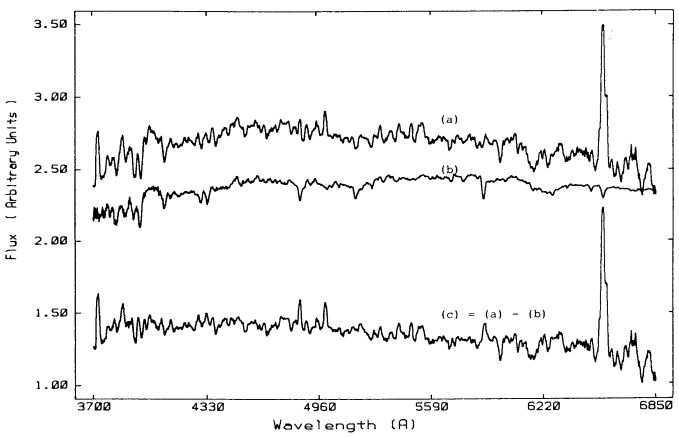

FIG. 9.—Subtraction of the stellar population from the 8″ south spectrum. (*a*) the observed spectrum; (*b*) the population template; (*c*) the subtraction (*a*) − (*b*). Constants were added to the spectra; flux is in arbitrary units.

We would like to thank Eduardo Bica for helpful discussions and for providing us with the population templates; C. B. acknowledges a CNPq fellowship; we would also like to thank an anonymous referee for valuable suggestions.

REFERENCES

Baldwin, J. A., Phillips, M. M., and Terlevich, R. 1981, *Pub. A.S.P.*, **551**, 5.
Bevington, P. R. 1969, *Data Reduction and Error Analysis For The Physical Sciences* (New York: McGraw-Hill).
Bica, E. 1988, *Astr. Ap.*, **195**, 76.
Cutri, R. M., Rudy, R. J., Rieke, G. H., Takunaga, A. T., and Willner, S. P. 1984, *Ap. J.*, **280**, 521.
De Bruyn, A. G., and Sargent, W. L. W. 1978, *A.J.*, **83**, 1257.
De Robertis, M. M., and Osterbrock, D. E. 1984, *Ap. J.*, **286**, 171.
Dopita, M. A., and Evans, I. N. 1986, *Ap. J.*, **307**, 431.
Ferland, G. J., and Osterbrock, D. E. 1987, *Ap. J.*, **318**, 145.
Filippenko, A. V., and Halpern, J. P. 1984, *Ap. J.*, **285**, 458.
Grandi, S. A., and Phillips, M. M. 1980, *Ap. J.*, **239**, 475.
Koski, A. T. 1978, *Ap. J.*, **223**, 56.
Lyutyi, V. M. 1973, *Soviet Astr.*, **16**, 763.
———. 1977, *Soviet Astr.*, **21**, 655.
———. 1979, *Soviet Astr.*, **23**, 518.
Marshall, N., Warwick, R. S., and Pounds, K. A. 1981, *M.N.R.A.S.*, **194**, 987.
McCall, M. L. 1984, *M.N.R.A.S.*, **208**, 253.
Nandy, K., Thompson, G. I., Jamar, C., Monfils, A., and Wilson, R. 1975, *Astr. Ap.*, **44**, 195.
Osterbrock, D. E. 1978, *Phys. Scripta*, **17**, 285.
Pagel, B. E. J., and Edmunds, M. G. 1981, *Ann. Rev. Astr. Ap.*, **19**, 77.
Penfold, J. E. 1979, *M.N.R.A.S.*, **186**, 297.
Penston, M. V., Penston, M. J., Selmes, R. A., Becklin, E. E., and Neugebauer, G. 1974, *M.N.R.A.S.*, **169**, 357.
Peterson, B. M., Foltz, C. B., Byard, P. L., and Wagner, R. M. 1982, *Ap. J. Suppl.*, **49**, 469.
Rieke, G. H. 1978, *Ap. J.*, **226**, 550.
Seaton, M. J. 1979, *M.N.R.A.S.*, **187**, 73p.
Seyfert, C. K. 1943, *Ap. J.*, **97**, 28.
Stone, R. P. S., and Baldwin, J. A. 1983, *M.N.R.A.S.*, **204**, 347.
Ulvestad, J. S., Wilson, A. S., and Sramek, R. A. 1981, *Ap. J.*, **247**, 419.
Westin, B. A. M. 1984, *Astr. Ap.*, **132**, 136.
———. 1985, *Astr. Ap.*, **151**, 137.
Wilson, A. S., Baldwin, J. A., Sun, S. D., and Wright, A. F. 1986, *Ap. J.*, **310**, 121.

C. J. BONATTO and M. G. PASTORIZA: Instituto de Fisica, UFRGS, Porto Alegre, RS, Brazil, CEP 90049